EFFECTS OF CLOSURE STRESS ON FRACTURE MORPHOLOGY AND ABSOLUTE PERMEABILITY OF A SHEAR FRACTURED SANDSTONE

Sultan M. Al Enezi, Philip M. Halleck, and Avrami S. Grader

ABSTRACT

Understanding the mechanical properties of fractures is very important to understand how fractures affect single and multi-phase flow not only in petroleum reservoirs but also in many other fields. Morphology of the shear fracture and the effects of increasing the closure stress on fracture properties and hydraulic behavior were studied under dry condition using high resolution Micro-Computed Tomography (MCT). A cylindrical Berea Sandstone sample was cored parallel to bedding and placed in a Hoek cell at 3.4 MPa confining stress. End loading of 23.3 kN, with oriented shims at each end, produced shear fracturing parallel to the axis and along the bedding planes. Use of a stiff testing frame allowed controlled post-failure shear displacement of 0.5 mm. The pre-fracture and post-fracture corrected gas permeabilities at 10.3 kPa were 28.9 mD and 81.5 mD, respectively, an increase in permeability of three times. Absolute permeability by water flow was not conducted before fracturing to avoid saturating the core with liquid before fracturing. The absolute water permeability is 103 mD, about 20 mD greater than the corrected gas permeability. After increasing the confining pressure, absolute water permeability decreased from 103 mD at 10.3 MPa to 65 mD at 17.2 MPa. Fracture connectivity was decrease about 56% after increasing the confining pressure. Fracture properties are highly affected by increasing the closure stress. As expected, the properties of the shear fracture (volume of the fracture, aperture distribution, and surface area decrease with increasing the confining. Roughness facture and connectivity coefficient (EPC) increase with increasing the confining pressure. Roughness factor calculation showed that the fracture is highly deviated from parallel plate model and applying cubic law is not valid to estimate the differential pressure during single-phase flow, it underestimated the differential pressure and hence will overestimate the permeability of the fracture.

INTRODUCTION

Shear fractures are the result of stresses that tend to slide one part of the rock past the adjacent part; they involve movement or displacement parallel to the plane of fracture. Gouge formation during shear fracturing makes it much more difficult to deal with shear fractures than with tensile fractures. Understanding the mechanical properties of shear fractures is very important, not only in petroleum reservoirs but also in many other fields like hydrothermal and geothermal systems, ground water contamination, and nuclear waste repositories. In petroleum reservoirs, shear fractures could enhance the

permeability when the deformation is dominated by compression leading to shear fracturing. The permeability enhancement could be not as good as tensile cracks but may be better than matrix permeability. Shear fractures can also act as no-flow reservoir boundaries. Shear fractures can be induced due to depletion and well-bore stress concentration. Shear fracture in this case will induce positive or negative skin problem.

Yeo *et al.* [1] studied the effect of shear displacement on the aperture and permeability of a rock fracture. They observed with increasing the displacement, the fracture became more permeable in the direction perpendicular to the shear displacement than in the direction parallel to the displacement. Makurat *et al.* [2] studied the effects of shear deformation on the permeability of natural rough joints. They have noticed significant increase in the conductivity with increasing shear displacement. Teufel [3] found that due to the formation of gouge zones and due to progressive decrease in grain size and porosity of the gouge zones with increasing shear displacement, the permeability across a shear fracture decreased with increasing the shear displacement.

Mohammad [4] and Al Enezi [5] used X-ray CT to study the effects of shear fractures diagonally induced in cylindrical Berea sandstone plug samples. In case of Mohammad's the fluid flow axis was perpendicular to the bedding planes while in Al Enezi's case the fluid flow axis was parallel to bedding planes. In both cases, the fractures were induced diagonal to the fluid flow axis. Contrary to the earlier study [4], Al Enezi found a reduction in the absolute permeability by about 30% after fracturing. There were significant differences between the results of both studies, which could be either due to the direction of the fracture relative to the bedding plane, or could be due to the complexity of the induced shear fracture. Al Enezi [6] studied the effects of the direction of the induced shear fracture relative to the bedding plane and the magnitude of the displacement on absolute permeability. Two samples were cut perpendicular to the bedding plane and two were cut parallel to the bedding plane. Generally speaking, the fracture increased the absolute permeability. In the parallel case, increasing the fracture displacement increased the connectivity of the fracture and its absolute permeability (relative to the non-displaced case). In the perpendicular case, fracture displacement reduced the connectivity and its absolute permeability.

This study applied X-ray micro CT scanning to determine the nature and behavior of a shear fracture induced parallel to fluid flow path in a Berea Sandstone under different closure stresses. A modified shear fracturing procedure was applied to induce the fracture parallel to the fluid flow axis. Pre-fracturing and post-fracturing absolute permeabilities were measured to determine the effects of shear fracture on single-phase flow behavior. The results of this study will be a building block for further experimental and works to understand the role of shear fractures on multi-phase flow in porous media.

Experimental Method
Layered Berea sandstone sample was jacketed in heat shrinkable Teflon to keep the gouge and matrix intact after fracturing. To create a shear fracture parallel to the bedding

planes and parallel to the fluid flow axis, the sample was shimmed using half circles of wood and metal pieces. Then the sample was loaded in the Hoek cell and confining pressure of 1500 psig (10.3 MPa) was applied. The pressurized Hoek cell was mounted inside the stiff testing machine and axial compression force was applied at a displacement rate of 0.003 mm/sec. After failure, the sample was displaced an additional 0.50 mm. The fractured Berea sample was surface ground then loaded inside a high-pressure aluminum/fiber composite core holder. The core holder was mounted inside the scanner and it was not moved out during the experiment. Absolute permeability was measure and CT images were acquired at to different confining pressures 1500 psig and 2500 psig.

RESULTS AND DATA ANALYSIS

Fracture Characterization

Based on the difference between the CT numbers of the fracture and the matrix, fractures were extracted at both confining pressure conditions. Figure **1** shows that there are two fractures initiated from the top and the bottom of the sample, propagated toward the center. This hypothesis is supported by simulating the fracturing process using finite element analysis (FEA). The young's modulus (E) of 23800 MPa and Poisson's ratio (v) of 0.19 at 40 MPa confining pressure was assigned for the rock block (NER)[7]. As shown in Figure **2**, loads were applied over opposite halves of the bottom and top of the sample. The maximum xy-shear force distribution occurs at the top and bottom of the core sample suggesting that these two points are the most likely areas to initiate the fracture. FE modeling results are in agreement with the experimental results and confirmed that resulted shear fracture initiated in the top and bottom of the sample then propagated toward the center of the sample.

Effects of Closure Stress on Fracture Properties

Properties of the fracture like volumes, asperities, average apertures, surface area and surface-to-volume ratio were calculated at both closure conditions by using the CT images and combining commercial image processing software and some PV-Wave programs. Table **1** shows the results of the fracture properties at two different confining pressures. After increasing the confining pressure to 2500 psig, the fracture volume was reduced to 191 mm^3, a 30% reduction. The 2-D aperture maps of the fracture at both closure stresses, Figure **3**, shows that the fracture is more connected and has smaller number of large asperities at 1500 psig than at 2500 psig confining pressure. The asperity ratio increased from 19% to 33% after increasing the confining pressure. Fracture volume and surface area were both reduced after increasing the confining pressure by similar percentages, thus keeping the surface-to-volume ratio constant. Figure **4** shows that there is there is a shift to the left (smaller apertures) after increasing the confining pressure, which indicates a reduction in average aperture.

Roughness factor was calculated using the fracture aperture distribution. Zimmerman *et al.* [8] defined the roughness factor as the ratio of the standard deviation and the average mechanical aperture of the fracture. As the calculated roughness factor increases, the validity of parallel plate model should decrease. The result showed that the roughness

factor increases as confining pressure increases indicating an increase in the rugosity of the fracture. Assuming that the fracture surfaces themselves do not change, the major cause of the incremental roughness is actually the reduction in the aperture.

Witherspoon *et al.* [9] used the parallel plate approximation to determine the pressure drop along fracture during single-phase flow using the cubic law. The experimental differential pressure measured during injecting the oil with a flow rate of 2 cc/min was 0.6 atm while the estimated differential pressure applying cubic law was 0.018 atm. the fracture is highly deviated from parallel plate model and applying cubic law is not valid to estimate the differential pressure during single-phase flow, it underestimated the differential pressure and hence will overestimate the permeability of the fracture.

To measure the connectivity of the fracture, the Euler-Poincare Coefficient (EPC), summarized by Odgaard *et al.* [10], was calculated. An increase in EPC at high confining pressure was observed. The increase in EPC is a consequence of creating new asperities. To address the relationship between EPC and average aperture in more details, the fracture was divided into small regions (Figure **5**). Average Aperture and EPC were calculated for each region separately. Figure **6** summarize the average aperture and EPC calculations for the selected regions. It is clear that EPC has an excellent relation with the average aperture, as the average aperture decreases, the EPC number increases. Brine absolute permeability shows 35% reduction after increasing the confining pressure.

CONCLUSIONS

Increasing the confining pressure reduced the absolute permeability by about 35%, Roughness factor calculations at both closure stresses showed a deviation from parallel plate model. Measurement of absolute permeability and fracture aperture confirm the invalidity of the cubic law to predict absolute permeability of shear fractures. Surface-to-volume ratios were similar at both confining pressures, suggesting that fracture connectivity relies more on fracture aperture and asperities area than on the surface-to-volume ratio. As anticipated, the properties of the shear fracture (volume of the fracture, aperture distribution, asperities ratio, surface area, roughness facture, and connectivity density) decrease with increasing the confining pressure. EPC number could be used as a parameter to describe the connectivity of the fracture.

REFERENCES

1- Yeo, I. W., DE Freitas, M. H., Zimmerman, R. W. "Effect of Shear Displacement on the Aperture and Permeability of a Rock Fracture." Int. J. Rock Mech. Min. Sci. & Geomech. Abstr., 1998 **35**: 1051-1070.
2- Makurat, A. "The Effect of Shear Displacement on the Permeability of Natural Rough Joints." IProceeding of the 17th International Congress of the International Association of Hydrogeologists, 1985 **39**: 99-106.
3- Teufel, L. W"Permeability Changes during Shear Deformation of Fractured Rock." Proceeding of the 28th U.S. Symposium on Rock Mechanics, 1987. **29**: 473-480.
4- Mohammad, Nazia. "Effects of Artificial Shear Fracture on Two-Phase Flow in Berea Sandstone." Ms. Thesis, Pennsylvania State University, 2004.

5- Al Enezi, S. " Two Phase Flow in a Shear Fracture in a Layered Sandstone". MS Thesis, Pennsylvania State University, 2005.

6- Al Enezi, S., Grader A., Halleck P." Effects of Shear-Fracture Displacement and Orientation on Fracture Topology and Absolute Permeability". SCA 2007.

7- New England Research, Inc. / 802-296-2401 / info@ner.com / www.ner.com.

8- Zimmerman, R. W., Kumar, S. and Bodvarsson, G. S. "Lubrication theory analysis of the permeability of rough-walled fractures." Int. J. Rock Mech. Min. Sci. & Geomech. Abstr., 1991 **28(B12)**: 325-331

9- Witherspoon, P. A., Wang, J. S. Y., Iwai, K., Gale, J. E. (1980), Validity of Cubic Law for Fluid Flow in a Deformable Rock Fracture, *Water Resources Research*, *16*, 1016-1024.

10- Odgaard, A. and Gundersen, H. "Quantification of Connectivity in Cancellous Bone, with Special Emphasis on 3-D Reconstructions," **Bone,** 1993. **14**: 173-182.

Table 1: Fracture properties at different confining pressures

Closure Pressure, psig	1500	2500	Change, %
Fracture Volume, mm^3	275	191	-31
Average Aperture, mm	0.227	0.192	-15
Asperities Ratio, %	19	33	+ 74
Surface Area, mm^2	5500	3900	-29
S/V Ratio	20	20	0
Absolute Perm, mD	102	64	-37
Conductivity, cc/sec/atm	0.25	0.11	-56
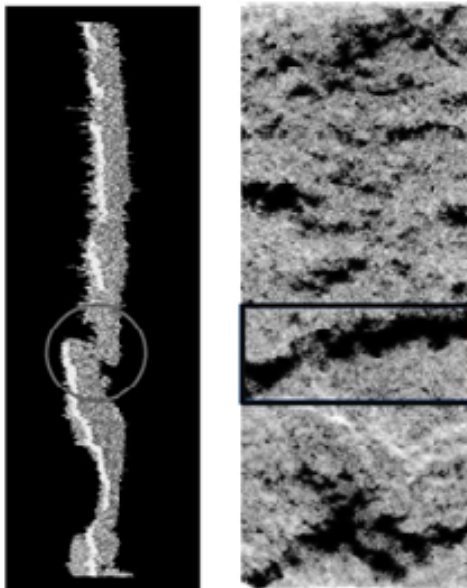
Figure **1**: 3-D fracture map (left) and 2-D aperture map (right) show two main fractures regions connected in the center.
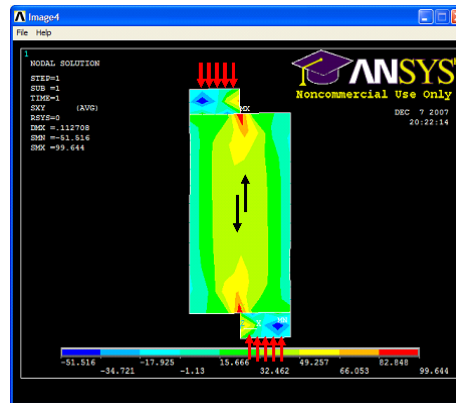
Figure **2**: XY-shear stress distribution when axial load was applied. Red is the maximum and blue is the minimum shear stress.
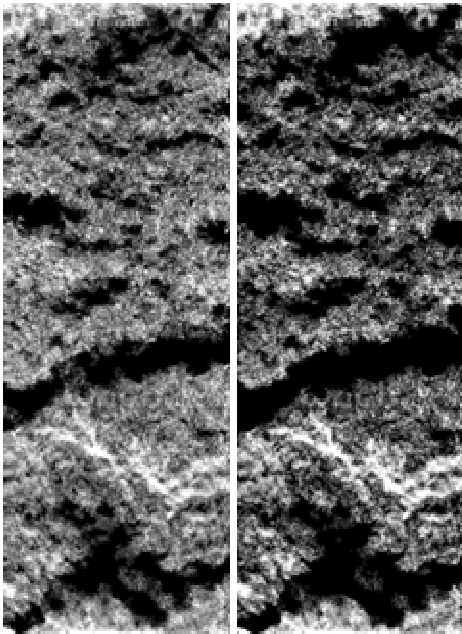
Figure **3**: 2-D aperture map (The linear gray scale is between 0 and 150 microns).
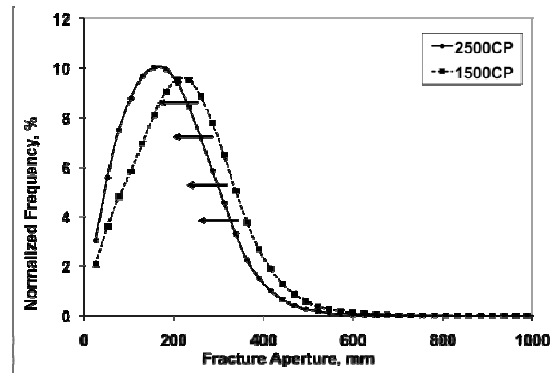
Figure **4**: Aperture Distributions at low confining pressure and high confining pressure .
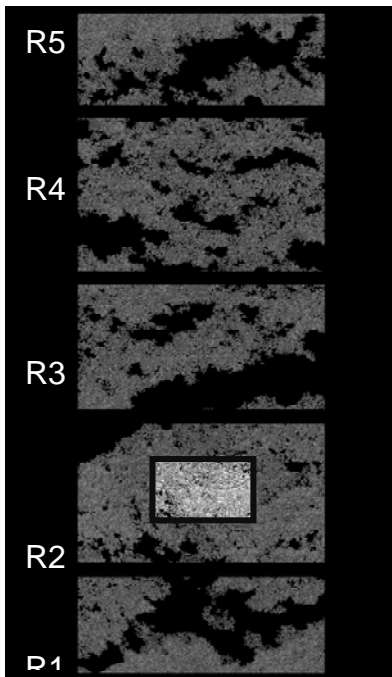
Figure **5**: The area inside the red box has the largest average aperture.
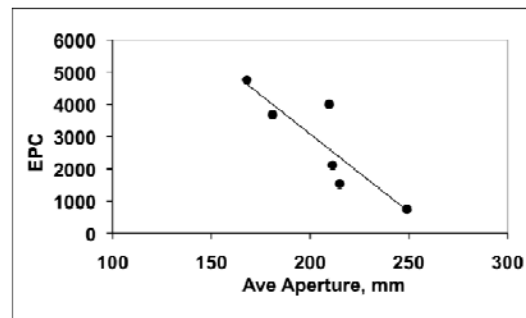
Figure **6**: Aperture distributions for discrete regions of the fracture at 2500 psig confining.